Measurement of the Inclusive Charm Cross Section at 4.03 GeV and 4.14 GeV

J. Z. Bai,[1] O. Bardon,[5] I. Blum,[10] A. Breakstone,[8] T. Burnett,[11] G. P. Chen,[1] H. F. Chen,[3] J. Chen,[4] S. J. Chen,[1] S. M. Chen,[1] Y. Chen,[1] Y. B. Chen,[1] Y. Q. Chen,[1] B. S. Cheng,[1] R. F. Cowan,[5] X. Z. Cui,[1] H. L. Ding,[1] Z. Z. Du,[1] W. Dunwoodie,[7] X. L. Fan,[1] J. Fang,[1] C. S. Gao,[1] M. L. Gao,[1] S. Q. Gao,[1] P. Gratton,[10] J. H. Gu,[1] S. D. Gu,[1] W. X. Gu,[1] Y. F. Gu,[1] Y. N. Guo,[1] S. W. Han,[1] Y. Han,[1] F. A. Harris,[8] J. He,[1] M. He,[6] D. G. Hitlin,[2] G. Y. Hu,[1] T. Hu,[1] X. Q. Hu,[1] D. Q. Huang,[1] Y. Z. Huang,[1] J. M. Izen,[10] C. H. Jiang,[1] S. Jin,[1] Y. Jin,[1] L. Jones,[2] S. H. Kang,[1] Z. J. Ke,[1] M. H. Kelsey,[2] B. K. Kim,[10] D. Kong,[8] Y. F. Lai,[1] H. B. Lan,[1] P. F. Lang,[1] A. Lankford,[9] F. Li,[1] J. Li,[1] P. Q. Li,[1] Q. Li,[6] R. B. Li,[1] W. Li,[1] W. D. Li,[1] W. G. Li,[1] X. H. Li,[1] X. N. Li,[1] S. Z. Lin,[1] H. M. Liu,[1] J. Liu,[1] J. H. Liu,[1] Q. Liu,[1] R. G. Liu,[1] Y. Liu,[1] Z. A. Liu,[1] X. C. Lou,[10] B. Lowery,[10] J. G. Lu,[1] J. Y. Lu,[1] S. Luo,[1] Y. Luo,[1] A. M. Ma,[1] E. C. Ma,[1] J. M. Ma,[1] R. Malchow,[4] M. Mandelkern,[9] H. S. Mao,[1] Z. P. Mao,[1] X. C. Meng,[1] H. L. Ni,[1] J. Nie,[1] S. L. Olsen,[8] J. Oyang,[2] D. Paluselli,[8] L. J. Pan,[8] J. Panetta,[2] F. Porter,[2] E. Prabhakar,[2] N. D. Qi,[1] Y. K. Que,[1] G. Rong,[1] M. Schernau,[9] B. Schmid,[9] J. Schultz,[9] Y. Y. Shao,[1] D. L. Shen,[1] H. Shen,[1] X. Y. Shen,[1] H. Y. Sheng,[1] H. Z. Shi,[1] E. Soderstrom,[7] X. F. Song,[1] J. Standifird,[10] D. Stoker,[9] F. Sun,[1] H. S. Sun,[1] S. J. Sun,[1] J. Synodinos,[7] Y. P. Tan,[1] S. Q. Tang,[1] W. Toki,[4] G. L. Tong,[1] F. Wang,[1] L. S. Wang,[1] L. Z. Wang,[1] M. Wang,[1] P. Wang,[1] P. L. Wang,[1] S. M. Wang,[1] T. J. Wang,[1] Y. Y. Wang,[1] M. Weaver,[2] C. L. Wei,[1] W. J. Wisniewski,[7] D. M. Xi,[1] X. M. Xia,[1] P. P. Xie,[1] D. Z. Xu,[1] R. S. Xu,[1] Z. Q. Xu,[1] S. T. Xue,[1] J. Yan,[1] W. G. Yan,[1] C. M. Yang,[1] C. Y. Yang,[1] H. Yang,[10] W. Yang,[4] M. H. Ye,[1] S. Z. Ye,[1] K. Young,[11] C. S. Yu,[1] C. X. Yu,[1] Z. Q. Yu,[1] C. Z. Yuan,[1] B. Y. Zhang,[1] C. C. Zhang,[1] D. H. Zhang,[1] H. L. Zhang,[1] J. Zhang,[1] J. W. Zhang,[1] L. S. Zhang,[1] S. Q. Zhang,[1] Y. Zhang,[1] Y. Y. Zhang,[1] D. X. Zhao,[1] H. W. Zhao,[1] J. W. Zhao,[1] M. Zhao,[1] W. R. Zhao,[1] J. P. Zheng,[1] L. S. Zheng,[1] Z. P. Zheng,[1] G. P. Zhou,[1] H. S. Zhou,[1] L. Zhou,[1] X. F. Zhou,[1] Y. H. Zhou,[1] Q. M. Zhu,[1] Y. C. Zhu,[1] Y. S. Zhu,[1] B. A. Zhuang,[1]

(BES Collaboration)

[1] *Institute of High Energy Physics, Beijing 100039, People's Republic of China*

[2] *California Institute of Technology, Pasadena, California 91125*

[3] *China's University of Science and Technology, Hefei 230026, People's Republic of China*

[4] *Colorado State University, Fort Collins, Colorado 80523*

[5] *Massachusetts Institute of Technology, Cambridge, Massachusetts 02139*

[6] *Shandong University, Jinan 250100, People's Republic of China*

[7] *Stanford Linear Accelerator Center, Stanford, California 94309*

[8] *University of Hawaii, Honolulu, Hawaii 96822*

[9] *University of California at Irvine, Irvine, California 92717*

[10] *University of Texas at Dallas, Richardson, Texas 75083-0688*

[11] *University of Washington, Seattle, Washington 98195*

(June 30, 1998)

The charm hadronic cross section at $\sqrt{s} = 4.03$ GeV and $\sqrt{s} = 4.14$ GeV has been measured at the Beijing Spectrometer. The measurement was made using 22.3 pb^{-1} of e^+e^- data collected at 4.03 GeV and 1.5 pb^{-1} of e^+e^- data collected at 4.14 GeV. Inclusive observed cross sections for the production of D^0 and D^+ and differential momentum spectra for D^0 and D^+ are presented at both energies. Observed cross sections were radiatively corrected to obtain tree level cross sections and R_D. A measurement of R was obtained from R_D and an extrapolation of R from below the charm threshold.

I. INTRODUCTION

The hadronic cross section of e^+e^- at all energies is needed to calculate the effects of vacuum polarization on parameters of the Standard Model. The energy region which contributes the largest uncertainty is the charm threshold region where the hadronic cross section has only been measured with an accuracy of $15-20\%$. Traditionally, σ_{hadron} is measured by examining all of the hadronic events in a given sample. This method requires a detailed understanding of trigger conditions, the efficiency of hadronic event selection criteria, and a subtraction of two photon events and other backgrounds. An alternative is measuring σ_{charm} and adding this to an extrapolation of the $\sigma_{u,d,s}$ contribution from the

region below charm threshold. The charmed mesons used in this study are the D^0 and D^+. The D_s cross sections are taken from earlier works. The charm counting method is intrinsically less sensitive to trigger conditions, beam-related backgrounds, and two photon backgrounds due to the distinctive topology of charmed meson events.

II. DATA SELECTION

The data used for this analysis were accumulated during 1992, 1993, and 1994 with the Beijing Spectrometer [2]. The total integrated luminosity at 4.03 (4.14) GeV was 22.3 (1.5) pb^{-1}. Candidate tracks were required to have a good track fit passing within 1.5 cm of the collision point in R and 15 cm in z, and satisfying $|\cos(\theta)| < 0.85$. Particle identification was achieved by using time of flight (TOF) and specific ionization energy (dE/dx). For pions, consistency ($CL(\pi) > 0.1\%$) and loose electron rejection ($L_\pi/(L_\pi + L_e) > 0.2$) were required where L_X is the likelihood for hypothesis X. Kaon identification required consistency ($CL(K) > 0.1\%$), pion rejection ($L_K/(L_K + L_\pi) > 0.5$) and loose electron rejection ($L_\pi/(L_\pi + L_e) > 0.2$). Multiple counting of D^0 candidates was removed by positively identifying pions using the selection ($L_K/(L_K + L_\pi) < 0.5$). Muons are rejected using a momentum dependent criteria based on track penetration into the muon detector.

III. D^0 AND D^+ SIGNAL

Inclusive $K^-\pi^+$ and $K^-\pi^+\pi^+$ invariant mass histograms are shown in Figures 1 and 2 for 4.03 GeV and for 4.14 GeV data respectively. Here and throughout this paper, reference to a state also implies its complex conjugate state. Each histogram was fit to a function which included a Gaussian signal plus a background function. For the $K\pi$ distribution, the background function consisted of a Gaussian centered at 1.60 GeV to describe $D^0 \to K\pi\pi^0$ decays plus a third order polynomial background. For the $K\pi\pi$ histogram, the background function consisted of a third order polynomial. The number of signal events in each mode is shown in Table I.

The momentum spectra of D candidates with a mass between 1.81 and 1.91 GeV is shown in Figure 3 for $\sqrt{s} = 4.03$ GeV. The three momentum regions near 0.15, 0.55, and 0.75 GeV correspond to $D^*\overline{D^*}$, $D^*\overline{D}$, and $D\overline{D}$ production respectively. The spectrum for $\sqrt{s} = 4.14$ GeV is shown in Figure 4. The momentum regions near 0.45 and 0.70 and 0.90 GeV correspond to $D^*\overline{D^*}$, $D^*\overline{D}$ and $D\overline{D}$ production respectively. The shapes of the $D^*\overline{D^*}$ spectrum and part of the $D^*\overline{D}$ spectrum are broadened due to Doppler-smeared D mesons coming from D^* decays. In addition, a small low momentum tail on each structure is expected due to initial state radiation. The background shape under the momentum spectrum is not flat, making a direct subtraction difficult.

IV. CROSS SECTION

If the reconstruction efficiency for D mesons were constant with respect to momentum, the observed cross section could be determined using

$$\sigma(e^+e^- \to DX) = \frac{N(\text{signal})}{\epsilon B \mathcal{L}} \qquad (1)$$

where N(signal) is the number of signal events, ϵ is the efficiency, B is the branching fraction of the D meson to a decay mode and $\mathcal{L}$ is the luminosity. Unfortunately, Monte Carlo studies show a momentum dependence to the reconstruction efficiency(Figure 5). In order to measure the cross section, the momentum spectrum for D^0 and D^+ mesons from 50 MeV to 850 MeV was divided into 10 MeV slices. For each momentum slice, the invariant mass distribution was fit with a Gaussian plus a polynomial background. The central value of the Gaussian was fixed. The width was fixed to a momentum dependent value determined by a fit to a coarser slicing of the data (Figure 6). The differential cross section with respect to momentum for this data is shown in Figure 7 and 8 for 4.03 GeV and 4.14 GeV respectively. The cross section times branching fractions of D^0 and D^+ mesons and cross sections calculated using the branching fractions of reference [1] are shown in Table II.

V. CORRECTIONS FOR INITIAL STATE RADIATION

The tree level cross section for charm at $\sqrt{s} = 4.03$ GeV and $\sqrt{s} = 4.14$ GeV was obtained by correcting the observed cross section for the effects of initial state radiation (ISR). The ISR correction is dependent on the cross section for all energies less than the nominal energy. Since this measurement was performed only at two energies, some theoretical modeling of the cross section distribution was

required. Two different theoretical predictions were used in this analysis, the Eichten Coupled Channel model [4], and a p-wave phase space formalism [?]. Each model gives the production cross section for each mode: $D\overline{D}$, $D\overline{D}^*$, and $D^*\overline{D}^*$. The correction for ISR was calculated for each production mode ($g_{\rm mode}$) separately as follows:

$$g_{\rm mode} = \frac{\sigma_{\rm obs,mode}}{\tilde{\sigma}_{B,\rm mode}} \tag{2}$$

where $\sigma_{\rm obs}$ for each mode is defined in terms of the tree level cross section ($\tilde{\sigma}_B$) for each mode as follows:

$$\sigma_{\rm obs}(s_{\rm nom}) = \int_0^1 dk \cdot f(k, s_{\rm nom})\tilde{\sigma}_B(s_{\rm eff}) \tag{3}$$

where $\tilde{\sigma}_B$ is the the tree level cross section as a function of the effective center of mass energy squared ($s_{\rm eff}$) which is defined as

$$s_{\rm eff} \equiv s_{\rm nom}(1-k) \tag{4}$$

where $kE_{\rm beam}$ is the energy of the radiated photons. The sampling function, $f(k, s_{\rm nom})$, represents a first order approximation of the effective luminosity of radiated photons as calculated from a two body radiation model. [5]

The number of D^0's in each production mode can be calculated as $N_{D^{*+}} \times B(D^{*+} \to D^0\pi^+) + N_{D^{*0}} + N_{D^0}$. The number of D^+'s in each mode can be calculated as $N_{D^{*+}} \times B(D^{*+} \to D^+X) + N_{D^+}$. The fractional cross section F_D for each production mode is calculated by dividing the product $N_D(\rm mode) \times \sigma_{\rm mode}(\rm obs)$ (the number of D's per mode times the observed cross section prediction) by the sum of the cross section predictions for all modes.

$$F_{D^0}(\rm mode) = \frac{N_{D^0}(\rm mode) \times \sigma_{\rm mode}(\rm obs)}{\sigma_{D^0}(\rm obs)} \tag{5}$$

$$F_{D^+}(\rm mode) = \frac{N_{D^+}(\rm mode) \times \sigma_{\rm mode}(\rm obs)}{\sigma_{D^+}(\rm obs)} \tag{6}$$

$$g(D^0) = \sum_{\rm modes} g(D^0, \rm mode) \times F_{D^0}(\rm mode) \tag{7}$$

$$g(D^+) = \sum_{\rm modes} g(D^+, \rm mode) \times F_{D^+}(\rm mode) \tag{8}$$

The ISR correction for D^0 and D^+ is calculated by adding the contributions from the six modes. The fractional cross sections for each mode are used as a weighting factor. Figure 9 shows the ISR correction for D^0, D^+, and D_s. The final correction for the production of initial state photons was calculated by averaging the correction calculated using the coupled channel model and its predicted fractional cross sections with the correction calculated using a phase space formula as shown in Figure 9. Since neither method models the data precisely, and the two models vary differently with energy, a systematic uncertainty is assigned to be one half the rms difference between the two models over the energy range 3.9 GeV to 4.2 GeV excluding the region from 4.021 to 4.027 where the Coupled Channel model $D\overline{D}$ cross section is tiny, causing the ISR correction to diverge. The corrections for initial state radiation at $\sqrt{s} = 4.03$ GeV and $\sqrt{s} = 4.14$ GeV are shown below:

$$4.03\,\text{GeV}: \; g(D^0) = 0.67 \pm 0.05 \tag{9}$$

$$g(D^+) = 0.73 \pm 0.05 \tag{10}$$

$$4.14\,\text{GeV}: \; g(D^0) = 0.83 \pm 0.06 \tag{11}$$

$$g(D^+) = 0.84 \pm 0.06 \tag{12}$$

The ISR correction for D_s mesons was calculated using the Coupled Channel model and the same p-wave phase space formalism that was used for D mesons. Figure 10 shows a prediction for the tree level cross section of D_s and D_s^*, the observed cross section of D_s and D_s^*, the fraction of D_s mesons from direct production, and the fraction of D_s mesons from D_s^* decays. Figure 9c shows the correction for initial state radiation for D_s mesons. The ISR contribution to the systematic error production for D_s is taken to as one half the RMS difference between the two models.

$$4.03\,\text{GeV}: \; g(D_s) = 0.73 \pm 0.04 \tag{13}$$

$$4.14\,\text{GeV}: \; g(D_s) = 0.78 \pm 0.05 \tag{14}$$

The ISR corrections are applied to the observed D^0 and D^+ cross sections to obtain the tree level cross section for D^0 and D^+ at 4.03 GeV and 4.14 GeV as shown below:

$$4.03\,\text{GeV}: \; \sigma_{D^0} = 20.9 \pm 0.6\,\text{nb} \tag{15}$$

$$\sigma_{D^+} = 6.7 \pm 0.3\,\text{nb} \tag{16}$$

$$4.14\,\text{GeV}: \; \sigma_{D^0} = 14.1 \pm 3.0\,\text{nb} \tag{17}$$

$$\sigma_{D^+} = 2.7 \pm 1.3\,\text{nb} \tag{18}$$

The BES observed D_s cross section at 4.03 GeV is $\sigma_{D_s^+D_s^-} = 0.31 \pm 0.06 \pm 0.10$ nb [3]. Applying the radiative correction, the tree level D_s cross section is $\sigma_{D_s^+D_s^-} = 0.42 \pm 0.08 \pm 0.14$ nb. Mark III has reported the observed D_s cross section at 4.14 GeV to be $\sigma_{D_s^+D_s^-} = 0.72 \pm 0.17 \pm 0.23$ nb [6]. Applying the radiative correction, the tree level D_s cross section is $\sigma_{D_s^+D_s^-} = 0.92 \pm 0.22 \pm 0.30$ nb.

VI. SYSTEMATICS

Several systematic checks were performed. First the number of events in the signal from Figs. 1, and 2 were compared to the sum of the events in the signal of each momentum slice as shown in Table III. They were found to be in good agreement for 4.03 GeV data, validating the slicing technique. The poorer agreement for the 4.14 GeV data set appears to be due to much lower statistics.

The analysis was repeated using wrong sign combinations ($K^-\pi^-, K^-\pi^-\pi^+$) to explore systematic bias from the slicing and fitting procedure. As expected, the structures which were so evident in the right sign spectra were absent in the wrong sign spectra. (Fig. 11). There was, however, a small excess when the $K^-\pi^-\pi^+$ spectrum is integrated.

$$(\sigma_{D^0} + \sigma_{\overline{D}^0})_{WS} = 0.29 \pm 0.21\,\text{nb} \quad (19)$$

$$(\sigma_{D^+} + \sigma_{D^-})_{WS} = 0.7 \pm 0.2\,\text{nb} \quad (20)$$

Both the data and the charged MC show a small excess that is not present in neutral decays. A much larger MC study would be required to prove whether the source is procedural, or if there is a small feed down from right sign channels into the wrong sign analysis. If the source of the excess is procedural, the MC efficiency calculation should correct for the effect in the data. In either case, no correction is required.

Systematic error in this analysis has several sources. The first systematic error is from the uncertainty of the integrated luminosity. Integrated luminosity is measured using wide angle Bhabhas. Fit parameters were varied to evaluate the second systematic uncertainty. The width of the momentum slices was varied from 10 MeV to 40 MeV. The range over which the fit was done was varied both symmetrically and asymmetrically from $1.65 < M < 2.05$ GeV to $1.75 < M < 1.95$ GeV. The order of the background polynomial was varied from 3 up to 7. The third systematic uncertainty is the monte carlo statistical error on the reconstruction efficiency. The fourth systematic uncertainty arises from the uncertainty of charm branching fractions compiled by the Particle Data Group [1]. The calculation of the correction for initial state radiation introduces a systematic uncertainty based on its uncertainty. The magnitude of the systematic uncertainties is shown in Table IV. Systematic uncertainties are added in quadrature.

The total observed D^0 and D^+ cross sections are shown in Table V. Tree level D^0 and D^+ cross sections are shown in Table VI.

VII. TOTAL INCLUSIVE CHARM CROSS SECTION

Since all D mesons are produced in pairs, the tree level non-strange D cross section is shown as follows:

$$4.03\,\text{GeV}: \sigma(D\overline{D}X) = 0.5 \times (\sigma_{D^0} + \sigma_{\overline{D}^0} + \sigma_{D^+} + \sigma_{D^-}) = 13.8 \pm 0.5 \pm 1.6\,\text{nb} \quad (21)$$

$$4.14\,\text{GeV}: \sigma(D\overline{D}X) = 0.5 \times (\sigma_{D^0} + \sigma_{\overline{D}^0} + \sigma_{D^+} + \sigma_{D^-}) = 8.5 \pm 2.2 \pm 1.4\,\text{nb} \quad (22)$$

Adding the tree level D cross section to the tree level D_s cross section gives the total tree level charm cross section:

$$4.03\,\text{GeV}: \ \sigma_{\text{charm}} = 14.2 \pm 0.5 \pm 1.6\,\text{nb} \quad (23)$$

$$4.14\,\text{GeV}: \ \sigma_{\text{charm}} = 9.4 \pm 2.4 \pm 1.7\,\text{nb} \quad (24)$$

These results are compared to coupled channel model predictions in Table VI.

VIII. SUMMARY

The BES experiment has made a measurement of the observed cross section times branching fraction of the D^0 and D^+ at 4.03 GeV and 4.14 GeV. The $\sigma \cdot B$ values from this measurement are compatible with previous measurements by Mark I and Mark II as shown in Figure 12.

A measurement of R_D can be made by dividing σ_{charm} by the QED prediction for the tree level muon pair cross section

$$\sigma(e^+e^- \to \mu^+\mu^-) = \frac{86.8\,\text{nb}}{s\,(\text{GeV})^2} \quad (25)$$

giving

$$4.03\,\text{GeV}: \ R_D = 5.31 \pm 0.19 \pm 0.60 \quad (26)$$

$$4.14\,\text{GeV}: \ R_D = 3.71 \pm 0.95 \pm 0.67 \quad (27)$$

The contribution to R from light quarks (u,d,s) R_{uds} is 2.5 ± 0.25 [7], independent of center of mass energy. This value was compiled from an average of the measurements of R below 3.77 GeV. The value of R is estimated using $R = R_D/2 + R_{uds}$ giving

$$4.03\,\text{GeV}: \ R = 5.16 \pm 0.10 \pm 0.55 \quad (28)$$

$$4.14\,\text{GeV}: \ R = 4.36 \pm 0.48 \pm 0.59 \quad (29)$$

These values are compatible with previous R measurements using total cross section and R_D techniques as shown in Figure 13.

We would like to thank the staffs of the BEPC accelerator and the Computing Center at the Institute of High Energy Physics (Beijing). This work was supported in part by the National Natural Science Foundation of China under contract No. 19290400 and the Chinese Academy of Sciences under contract No. KJ85 (IHEP); by the Department of Energy under contract Nos. DE-FG03-92ER40701 (Caltech), DE-FG03-93ER40788 (Colorado State University), DE-AC02-76ER03069 (MIT), DE-AC03-76SF00515 (SLAC), DE-FG03-91ER40679 (UC Irvine), DE-FG03-94ER40833 (University of Hawaii), DE-FG03-95ER40925 (UT Dallas); by the U.S. National Science Foundation Grant No. PHY9203212 (University of Washington).

---

[1] R.M.Barnet et al. Phys. Rev. *D54,1 (1996) updated in the 1997 off-year partial update for the 1998 edition.*
[2] J.Z. Bai, et al., Nucl. Ins. Meth. *A344, 319 (1994).*
[3] J.Z. Bai, et al., Phys. Rev. *D52, 3781 (1995).*
[4] E. Eichten, et al., Phys. Rev. *D21, 203 (1980).*
[5] G. Bonneau and F. Martin, Nucl. Phys. *B27*, 380-397 (1971).
[6] J. Adler, et al., Phys. Rev. Letts. *63, 1211 (1989).*
[7] M.W. Coles, et al., Phys. Rev. *D26, 2190 (1982).*

Mode	$E_{c.m.}$(GeV)	Events
$D^0 \to K\pi$	4.03	4174 ± 163
$D^+ \to K\pi\pi$	4.03	2341 ± 138
$D^0 \to K\pi$	4.14	249 ± 36
$D^+ \to K\pi\pi$	4.14	126 ± 31

TABLE I. Number of inclusive signal events for each mode.

	$\sqrt{s}$ = 4.03 GeV	$\sqrt{s}$ = 4.14 GeV
$\sigma \cdot B(D^0 \to K\pi)$	0.537 ± 0.015 nb	0.45 ± 0.10 nb
$\sigma \cdot B(D^+ \to K\pi\pi)$	0.449 ± 0.017 nb	0.21 ± 0.10 nb
σ_{D^0}	14.0 ± 0.4 nb	11.7 ± 2.5 nb
σ_{D^+}	4.9 ± 0.2 nb	2.3 ± 1.1 nb

TABLE II. The cross section times branching fraction of D^0 and D^+ and the cross section of D^0 and D^+ at 4.03 GeV and 4.14 GeV.

	4.03 GeV		4.14	
	Inclusive D	Sum of Slices	Inclusive D	Sum of Slices
D^0	4174 ± 163	4232 ± 114	249 ± 36	210 ± 46
D^+	2341 ± 138	2395 ± 94	126 ± 31	66 ± 33

TABLE III. Comparison of the number of events found from the inclusive mass fit and the sum of the events from invariant mass fits for the momentum slices

Source	4.03 D^0	4.03 D^+	4.14 D^0	4.14 D^+	4.04 D_s	4.14 D_s
MC statistics	5%	4%	5%	4%		
Luminosity	5%	5%	13%	13%		
Fit parameters	5%	5%	5%	5%		
Branching Fraction	3%	7%	3%	7%		25%
total (no isr)	9%	11%	15%	16%	25%	32%
ISR	7%	7.5%	6%	6%	6%	6%
total (w/ isr)	11%	13%	16%	17%	25%	33%

TABLE IV. Sources of systematic uncertainty.

	$\sqrt{s} = 4.03$ GeV	$\sqrt{s} = 4.14$ GeV
$\sigma \cdot B(D^0 \to K^-\pi^+)$	$0.537 \pm 0.015 \pm 0.048$ nb	$0.45 \pm 0.10 \pm 0.07$ nb
$\sigma \cdot B(D^+ \to K^-\pi^+\pi^+)$	$0.449 \pm 0.017 \pm 0.049$ nb	$0.21 \pm 0.10 \pm 0.03$ nb
σ_{D^0}	$14.0 \pm 0.4 \pm 1.3$ nb	$11.7 \pm 2.5 \pm 1.8$ nb
σ_{D^+}	$4.9 \pm 0.2 \pm 0.5$ nb	$2.3 \pm 1.1 \pm 0.4$ nb

TABLE V. The total observed D^0 and D^+ cross sections.

$\sqrt{s} = 4.03$ GeV	experiment	theory
σ_{D^0}	$20.9 \pm 0.6 \pm 2.3$ nb	17.2 nb
σ_{D^+}	$6.7 \pm 0.3 \pm 0.9$ nb	5.8 nb
σ_{D_s}	$0.44 \pm 0.08 \pm 0.11$ nb	0.80 nb
$\sigma_{\rm charm}$	$14.2 \pm 0.5 \pm 1.6$ nb	12.3 nb
$\sqrt{s} = 4.14$ GeV	experiment	theory
σ_{D^0}	$14.1 \pm 3.0 \pm 2.3$ nb	15.2 nb
σ_{D^+}	$2.8 \pm 1.3 \pm 0.4$ nb	4.6 nb
σ_{D_s}	$0.92 \pm 0.22 \pm 0.30$ nb	0.92 nb
$\sigma_{\rm charm}$	$9.4 \pm 2.4 \pm 1.7$ nb	10.8 nb

TABLE VI. Comparison of measured tree level cross sections with predictions of the Coupled Channel model.

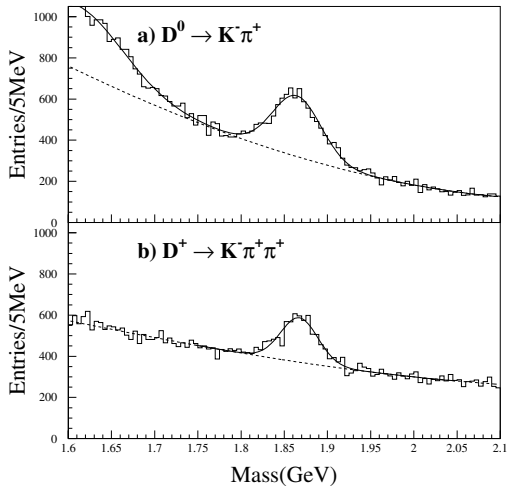

FIG. 1. The invariant mass of a) $K\pi$ and b) $K\pi\pi$ tags with momentum from 0 to 1 GeV at $E_{\rm c.m.} = 4.03$ GeV.

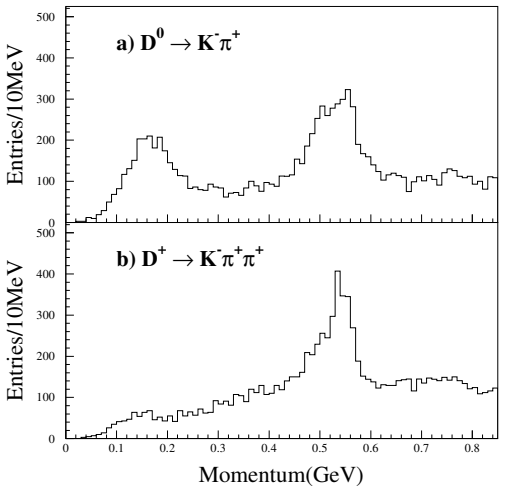

FIG. 3. The momentum of a) $K\pi$ and b) $K\pi\pi$ tags with a mass between 1.81 and 1.91 GeV at $E_{\rm c.m.} = 4.03$ GeV.

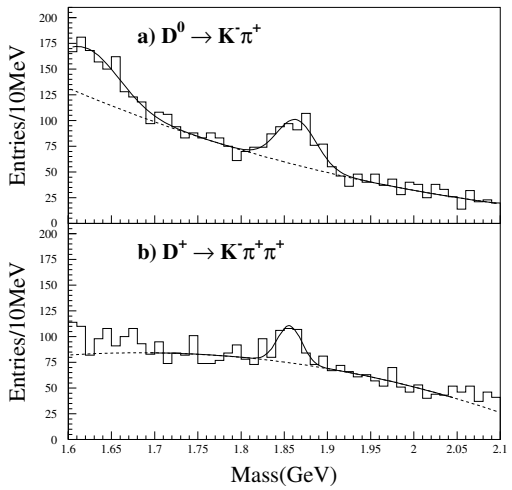

FIG. 2. The invariant mass of a) $K\pi$ and b) $K\pi\pi$ tags with momentum from 0 to 1 GeV at $E_{\rm c.m.} = 4.14$ GeV.

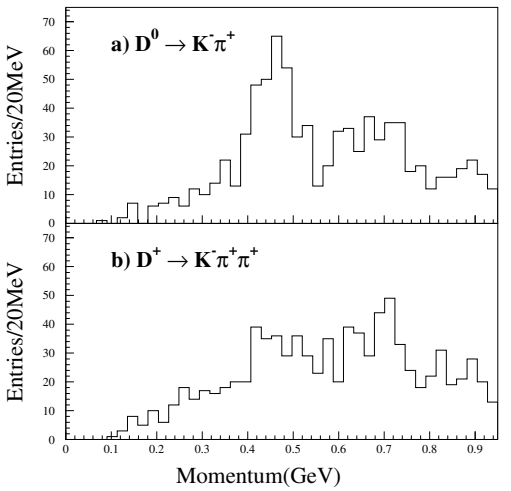

FIG. 4. The momentum of a) $K\pi$ and b) $K\pi\pi$ tags with a mass between 1.82 and 1.92 GeV at $E_{\rm c.m.} = 4.14$ GeV.

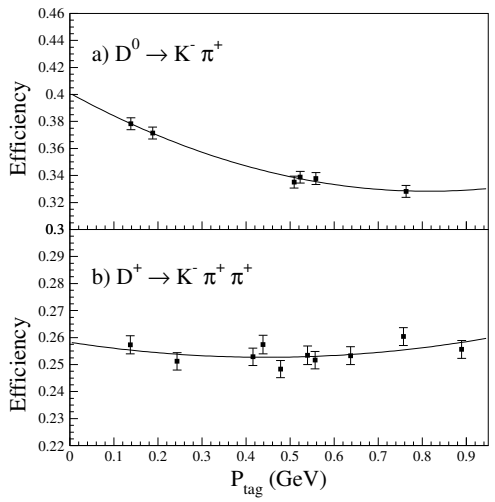

FIG. 5. The momentum dependence of the reconstruction efficiency.

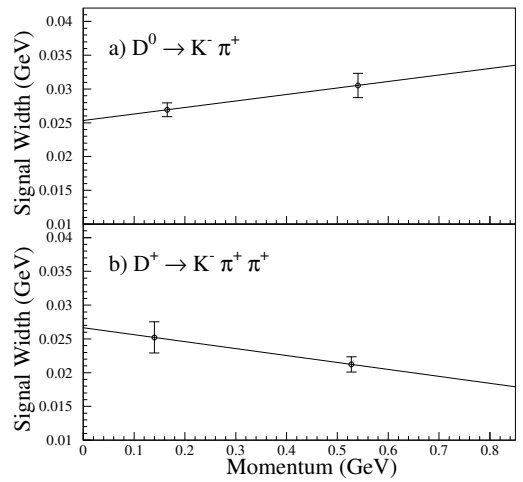

FIG. 6. The momentum dependence of the mass resolution.

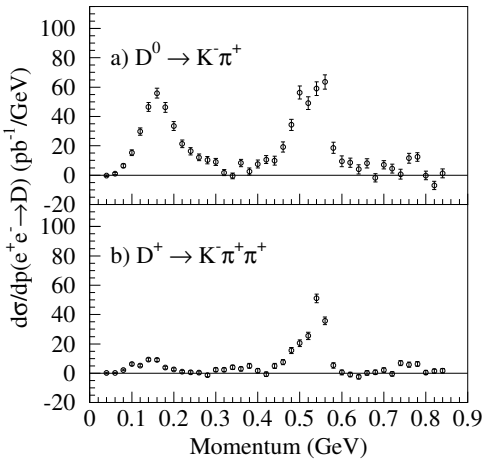

FIG. 7. The differential production cross section of $e^+e^- \to D^0 X$ versus the momentum of the tag at $E_{\rm c.m.} = 4.03$ GeV.

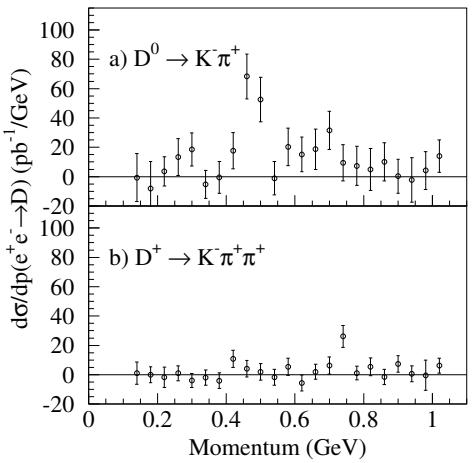

FIG. 8. The differential production cross section of $e^+e^- \to D^+ X$ versus the momentum of the tag at $E_{\rm c.m.} = 4.14$ GeV.

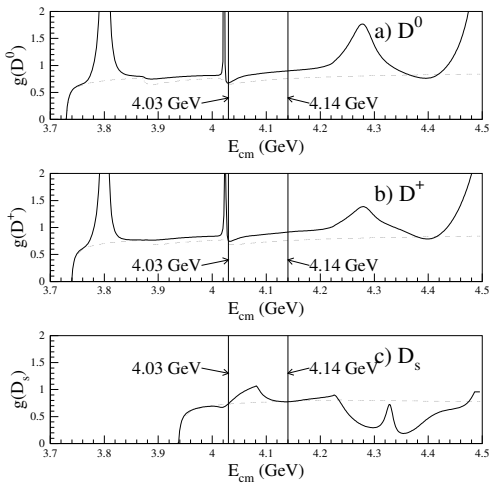

FIG. 9. The correction which adjusts the observed cross section to account for initial state radiations for a) D^0, b) D^+, and c) D_s. The correction using the Eichten coupled channel model is solid, while the p-wave phase space formalism is dashed.

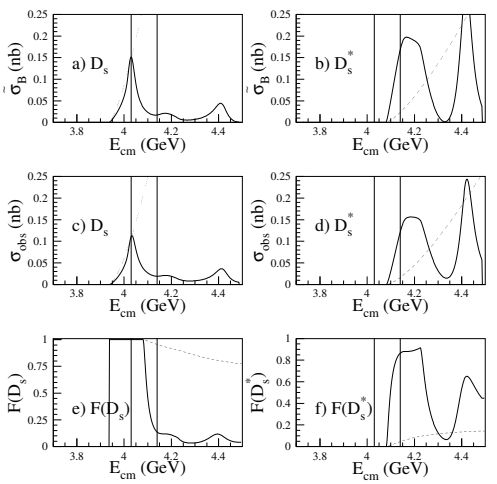

FIG. 10. a) The tree level cross section for D_s mesons. b) The tree level cross section for D_s^* mesons. c) The observed cross section for D_s mesons. d) The observed cross section for D_s^* mesons. e) The fraction of D_s mesons from direct production. f) The fraction of D_s mesons from D_s^* decay. The solid curve was obtained using the Coupled Channel Model. The dashed line was obtained using the p-wave phase space formalism.

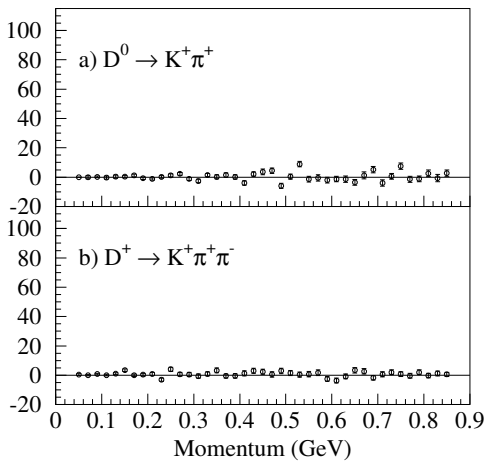

FIG. 11. The differential production cross section of the wrong sign background.

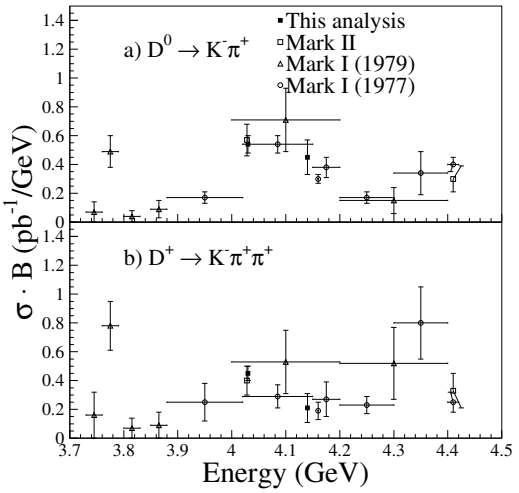

FIG. 12. A comparison of the observed integrated cross section times branching fraction for this analysis with those of Mark I and Mark II. a) $D^0 \to K\pi$, b) $D^+ \to K\pi\pi$.

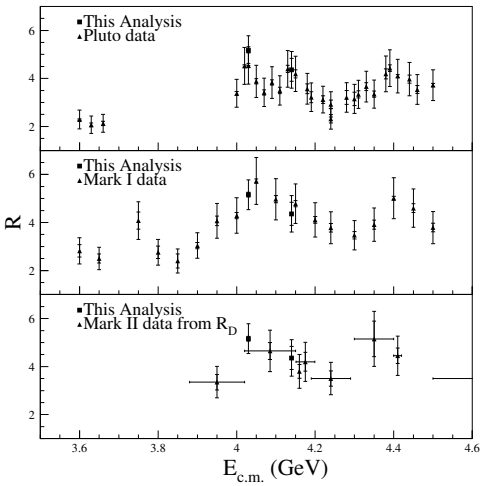

FIG. 13. A comparison of the value of R for this analysis with those of Pluto, Mark I and Mark II.